

Lateral Control of A Tailless Micro Aerial Vehicle

J. Hall*, D. Lawrence†, K. Mohseni‡

*Research and Engineering Center for Unmanned Vehicles,
Department of Aerospace Engineering,
University of Colorado, Boulder, CO 80309-429.*

A feedback controller is analyzed for a tailless Micro Aerial Vehicle (MAV) which is to be used for in-situ sensing of toxic plumes. The vehicle will be tube-launched for rapid deployment. The stability derivatives for the lateral dynamics of the aircraft are determined using a combination of Computational Fluid Dynamics and lifting line theory. The state-space model is found to be both completely reachable and completely observable. A standard feedback controller and state observer are implemented. Results show that the aircraft, which is initially unstable, can be controlled with the techniques proposed.

I. Introduction

Recent aircraft design has been focused on the development of Unmanned Aerial Vehicles (UAVs). These aircraft are capable of performing many of the roles that have traditionally been assigned to manned aircraft, but at less cost because the safety requirements are less strict. Additionally, advancements in miniaturization have led to the production of increasingly smaller components and systems. Micro Aerial Vehicles (MAVs) result from a fusion of the two technologies. MAVs are typically very small (~6 in. long), making them well suited for a variety of indoor and in-situ atmospheric sensing tasks.

This paper will present results obtained from simulations of a closed loop feedback controller and state observer designed for the MAV. The purpose of this paper is not to present a new technique for control; rather, this paper applies existing methods to a unique vehicle. The focus will be on the results of controller design for this particular aircraft. Section 1 will describe the motivation and design of the MAV, and give a brief overview of the vehicle dynamics. Section 2 presents the details of the state-space model and how it was obtained. Section 3 will describe the controller that was designed for the MAV, and present the results of simulated controller performance. Finally, Section 4 gives the concluding remarks.

A. Vehicle Design

The goal of the Colorado MAV project is to develop a MAV as a sensor platform for investigation of plumes of hazardous contaminants.¹ In the event of an industrial disaster or terrorist attack, dangerous chemicals and/or radioactive pollutants may be released into the lower atmosphere. The danger to public health and safety requires an expeditious response, especially in urban areas. However, the possibility of contaminants spreading over a large area or remaining in one region makes it difficult to initiate the proper procedures. Timely determination of toxin species, plume source and location, and prediction of plume evolution would improve the emergency response.² While there are many techniques that could be used for measuring the plume, including ground- and balloon-based sensors, MAVs have many qualities that make them well-suited for the task.³

*Graduate student, AIAA member.

†Associate Professor, AIAA Member

‡Assistant Professor, AIAA member.

Copyright © 2005 by the American Institute of Aeronautics and Astronautics, Inc. The U.S. Government has a royalty-free license to exercise all rights under the copyright claimed herein for Governmental purposes. All other rights are reserved by the copyright owner.

1. MAVs are operated remotely, thus avoiding additional human health risks.
2. MAVs have small mass, reducing the risk to people and property on the ground in the event of failure.
3. MAVs are more maneuverable than balloons and may be deployed to actively track the regions of highest contaminant concentration.
4. MAVs can be produced cheaply and operated by a small team, making it possible to deploy a large flock (~ 100 vehicles) at a reasonable cost.

B. Prototype Vehicle

Three of the most important factors contributing to the design of the MAV were the need for rapid launch of multiple vehicles, durability and cost effectiveness, and endurance. Accurately mapping of the toxic plume requires a flock of approximately 100 vehicles, which must be launched quickly after the plume is discovered. A tube launch concept was devised to store the vehicles prior to flight and assist in deployment. The vehicles would be folded to fit inside the tubes, and would reconfigure for flight after launch. Because of space requirements, the vertical tail was omitted from the MAV design. Additionally, by removing the vertical surfaces the MAV is less susceptible to damage. Since there are no landing gear for weight reasons, landings are performed by skidding on the aircraft's belly. Such landings would be likely to damage or destroy a vertical tail. The third reason for designing a tailless aircraft is a matter of efficiency. Vertical surfaces would be a significant source of drag without contributing to the lift.

The wings must fold or collapse to fit inside the tube. This is accomplished by pivoting the wings at the root and folding them back. After being ejected from the tube, the MAV would extend its wings and begin powered flight. A spring causes the wings to open. The same mechanism used to fold the MAV for storage is also used for in-flight morphing. During the high-speed egress to the contamination area the wings will move into a swept-back position. Upon reaching its destination, the MAV will decrease speed and the wings will move to their fully extended position, with a sweep angle of approximately 15° . By changing configuration for different speeds, the MAV will attain the maximum possible lift-to-drag ratio for every speed.³

In order to perform its task, the MAV must remain aloft for 1-2 hours. The energy requirements are a critical factor for achieving such duration, so the aircraft must be as efficient as possible.⁴ A high-aspect ratio wing was chosen to reduce the induced drag, and the Eppler 387 airfoil was selected for its performance at low Reynolds number.

The MAV is propelled by an electric motor which is mounted on the rear of the aircraft to make the vehicle more rugged. During landing the nose is often the first part of the aircraft to hit the ground, and a motor and propeller mounted there would be more likely to break. By placing the motor in the rear and using a folding propeller, it is less vulnerable. The batteries which power the motor and other electronics are stored in spars on the underside of the wings. This allows for a smaller fuselage and decreased bending moment at the root of the wing. The fuselage is designed to be just large enough to hold the avionics package and sensors, in keeping with the strategy of reducing the size of non-lifting components.

The MAV does not have a vertical surface for control. Instead, it uses elevons (elevator and aileron combination). The elevons deflect collectively to perform pitching maneuvers, and differentially for roll. Rather than having traditional control surfaces, which require hinge mechanisms that are both bulky and heavy, the MAV uses wing morphing. Servos connected directly to the wings twist the tips, achieving a motion similar to that of conventional ailerons. A prototype MAV is shown in Fig. 1. The focus of this paper is to determine whether elevons and two rate gyros (for roll and yaw) are enough to control the vehicle.

C. Flight Dynamics

A model for the aircraft dynamics is constructed using the standard procedure of linearizing the equations of motion for the aircraft. The stability derivatives are then evaluated for this particular aircraft, giving a state-space system of the form

$$\begin{aligned}\dot{\mathbf{x}} &= \mathbf{A}\mathbf{x} + \mathbf{B}\mathbf{u} \\ \mathbf{y} &= \mathbf{C}\mathbf{x} + \mathbf{D}\mathbf{u}\end{aligned}\tag{1}$$

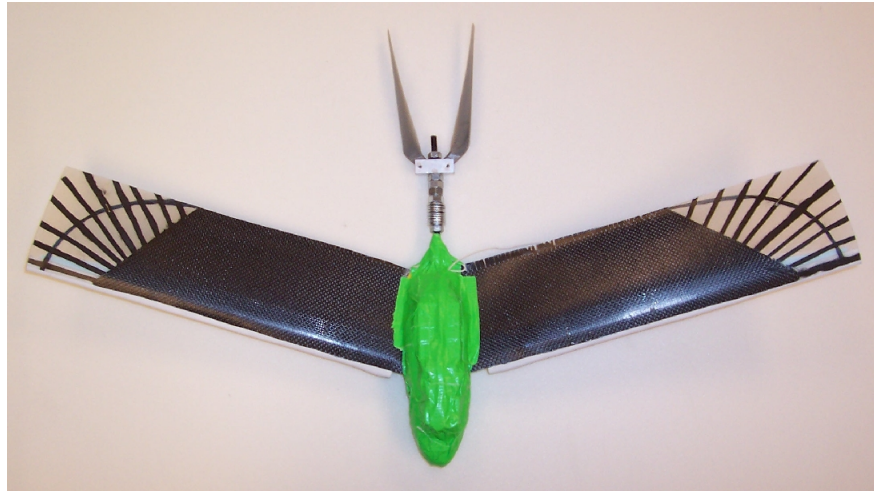


Figure 1. Second generation MAV design.

The dynamic behavior of an aircraft is governed by Newton's equations of motion, which relate the vehicle's linear and angular accelerations with the forces and moments acting on it. In general, there are six degrees of freedom – translation in the x , y , and z directions, as well as rotation about the x , y , and z axes – with twelve corresponding variables – position and velocity for each degree of freedom. The six equations thus obtained describe a relationship between the force and couple system (which is a function of the aircraft's orientation and velocity) applied to the aircraft and its acceleration.

The orientation of the aircraft is related to an inertial frame of the earth by Euler angles.⁵⁶ The yaw angle ψ , the pitch angle θ , and the roll angle ϕ describe rotations about the z -, x -, and y -axes, respectively. The position of the aircraft is described in terms of earth-fixed coordinates x_f , y_f , and z_f . The equations which relate position and velocity measured in the aircraft frame to those measured in the fixed frame are called kinematic transformation equations and supply the remaining six equations.

Newton's equations and the kinematic transformation equations are now combined to form a system describing how the aircraft moves when forces and moments are applied. However, these forces and moments depend on the motion of the aircraft. The relationship between the aerodynamic force system and the aircraft's motion is quite complex and nonlinear in the general form. By considering only small disturbances from a reference state the equations may be reduced to a linear system. The linearization involves retaining the constant and linear terms of a Taylor series expansion to approximate a given function. A nonlinear function f of two variables x and y may be approximated as

$$f(x, y) \cong f(x_0, y_0) + \frac{\partial f}{\partial x}(x_0, y_0)(x - x_0) + \frac{\partial f}{\partial y}(x_0, y_0)(y - y_0) \quad (2)$$

This technique is then applied to the nonlinear system governing the aircraft's motion. By analysis of order of magnitude and the observation that the aircraft is symmetric about the x - z plane, as well as practical insight about the relationships between the forces and kinematic variables, further simplifications can be made. For example, a yaw to the right should have the same effect on pitching moment as an equal yaw to the left. This means that the pitching moment is an even function of yaw, and its derivative evaluated at the reference state (yaw equal to zero) vanishes. One convenient result of these simplifications is a decoupling of the longitudinal and lateral modes, which can be constructed as two systems independent of each other.

There are six variables for the lateral dynamics: sideslip velocity v , roll rate p , yaw rate r , lateral position y_f , and the two Euler angles ϕ (roll angle) and ψ (yaw angle). Additionally, F_{y_b} is the lateral force (in the y -direction) applied to the vehicle, M_{x_b} is the roll moment, and M_{z_b} is the yaw moment. The final variable is the input, which is a differential aileron displacement δ_a for this aircraft. The resulting linear set of equations for the lateral dynamics of the aircraft is given below.

$$\begin{aligned}
& \begin{bmatrix} W/g & 0 & 0 & 0 & 0 & 0 \\ 0 & I_{xxb} & -I_{xz_b} & 0 & 0 & 0 \\ 0 & -I_{xz_b} & I_{zz_b} & 0 & 0 & 0 \\ 0 & 0 & 0 & 1 & 0 & 0 \\ 0 & 0 & 0 & 0 & 1 & 0 \\ 0 & 0 & 0 & 0 & 0 & 1 \end{bmatrix} \begin{bmatrix} \dot{v} \\ \dot{p} \\ \dot{r} \\ \dot{y}_f \\ \dot{\phi} \\ \dot{\psi} \end{bmatrix} \\
= & \begin{bmatrix} F_{y_b,v} & F_{y_b,p} & F_{y_b,r} - V_0 W/g & 0 & W \cos(\theta_0) & 0 \\ M_{x_b,v} & M_{x_b,p} & M_{x_b,r} & 0 & 0 & 0 \\ M_{z_b,v} & M_{z_b,p} & M_{z_b,r} & 0 & 0 & 0 \\ 1 & 0 & 0 & 0 & 0 & V_0 \cos(\theta_0) \\ 0 & 1 & \tan(\theta_0) & 0 & 0 & 0 \\ 0 & 0 & \sec(\theta_0) & 0 & 0 & 0 \end{bmatrix} \begin{bmatrix} v \\ p \\ r \\ y_f \\ \phi \\ \psi \end{bmatrix} + \begin{bmatrix} F_{y_b,\delta_a} \\ M_{x_b,\delta_a} \\ M_{z_b,\delta_a} \\ 0 \\ 0 \\ 0 \end{bmatrix} \delta_a \quad (3)
\end{aligned}$$

II. Aerodynamic Model

Body-fixed axes are used to describe the aircraft's motion. The x -axis is chosen to be the direction of motion for level, steady flight. This means that if the MAV flies at an angle of attack α during level flight, the x -axis is rotated downward by α from the axis of the fuselage. The z -axis points downward perpendicular to $\hat{\mathbf{x}}$. Based on the above choice for the x -axis, $\hat{\mathbf{z}}$ is aligned with the gravity vector. The y -axis is chosen to complete the right-handed coordinate system, hence pointing horizontally to the right.

The matrix given in Eq. (3) above is singular. By inspection it is determined that the variables y_f and ψ do not contribute to the dynamics of the system, so they are removed from the system without affecting its behavior.

To evaluate the coefficients in the A matrix, a combination of methods are used. First, the sideslip velocity v is replaced by the sideslip angle β , defined as the angle between the aircraft's plane of symmetry and the velocity vector. For the β derivatives, which depend only on the direction of flow and not its rate of change, numerical simulations are used to find the forces and moments at different values of β . The derivatives are evaluated by applying a backward difference. The other coefficients depend on the angular velocity of the aircraft and are not possible to obtain via simulation. Instead, lifting line theory is applied to the MAV.

A. Computational Fluid Dynamics

Numerical flow simulations are used to evaluate the β derivatives. To simulate the flow around the MAV, the flow solver Argo is used on an eight-processor parallel computer. The CFD software is a domain decomposition-based parallel three-dimensional flow solver with capabilities for both the Euler and Navier-Stokes equations. An unstructured tetrahedral mesh is used with dual control volumes. The solver uses a combination of finite volumes and finite elements for the spatial discretization. The AUSM flux function, with a freestream Mach number of 2.9×10^{-2} , is used for the convective terms.⁷ Temporal discretization is accomplished with an upwind scheme for the convective term and a Galerkin method for the diffusive term. The flow is integrated in time with a backward Euler scheme.

To solve the system of nonlinear equations, a series of nonlinear and linear iterations are performed. The goal of the iterative process is to drive the global norm of the residual to zero, thus ensuring that the governing equations are satisfied. A Newton-Krylov method is employed for the nonlinear iteration. At each step in the Newton-Krylov method, a linear system is solved using the GMRES algorithm with RAS preconditioning.⁸ Output is generated as a post-processing step within the main code, and includes the flow variables for the entire domain as well as forces and moments for selected surfaces. The forces and moments are the key ingredient for constructing the state-space model.

The process begins with generating a CAD model of the MAV. The model is designed to capture the essential features of the prototype for the MAV (Fig. 2(a)).

The CAD model is used to create a cavity in a much larger sphere. This sphere forms the computational domain. Next, the mesh generator is used to create an unstructured mesh. Triangular elements are first

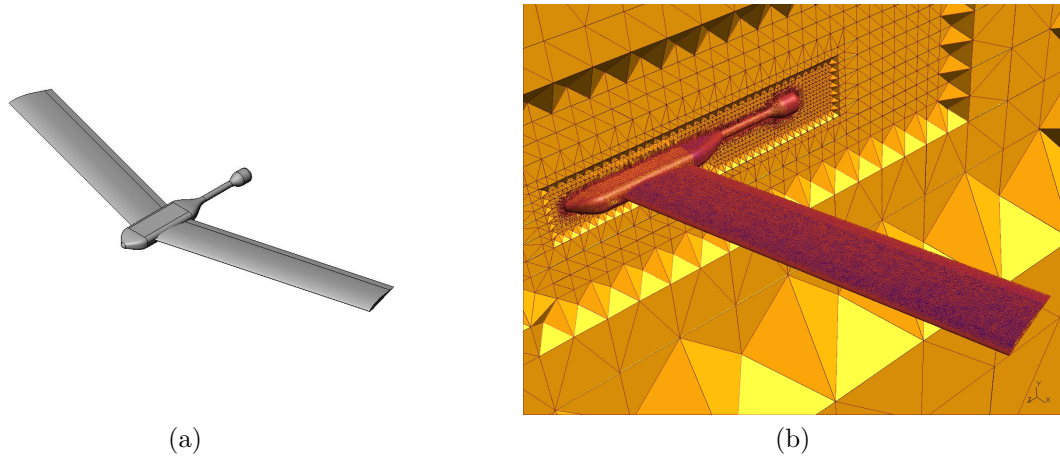


Figure 2. (a) CAD model of the MAV. (b) Cut through center of computational domain showing mesh.

used to discretize the surfaces of the vehicle. The surface mesh is then refined in areas of high curvature, such as the leading edges of the wings. Stretched tetrahedral elements are now formed near the surface of the vehicle to capture the effect of the boundary layer. The remaining volume is filled with tetrahedra. Finally, the mesh is refined in cylinders and cuboids to more accurately capture the effects of tip vortices and the wake behind the vehicle. The resulting mesh has approximately one and a half million nodes and nine million elements.

Steady-state computations are performed in two stages to obtain the flow around the MAV and the system of forces acting upon it. The first computation employs a constant reconstruction of flow variables within the elements. Nonlinear newton iterations are performed until the global norm of the residual decreases by 10 orders of magnitude. The final flow field is then used as the initial condition for a computation with linear reconstruction of the flow variables. The second computation is terminated when the global norm of the residual decreases by six orders of magnitude, or when 50 nonlinear iterations are completed. Five simulations are performed at sideslip angles of 0° , $\pm 2^\circ$, and $\pm 4^\circ$. The net forces and moments in the x -, y -, and z -directions are obtained for each case. The lateral force F_{y_b} , roll moment M_{x_b} , and yaw moment M_{z_b} are plotted versus yaw angle β . A least squares fit is then applied to each data set, and the slope of the fitting curve yields the derivatives $F_{y_b,\beta}$, $M_{x_b,\beta}$, and $M_{z_b,\beta}$.

B. Lifting Line Theory

Classical lifting line theory is used to evaluate the stability derivatives with respect to roll rate p and yaw rate r . The technique involves superposing vortices of various strengths on the wing and its wake. By combining a large number of vortices it is possible to compute the induced drag.

When an aircraft rolls, one wing experiences an increase in the relative angle of attack, while the other experiences a decrease. A differential of lift and induced drag results, causing yaw and roll moments. By accounting for the change in relative angle of attack, the lift and induced drag on each wing may be determined from lifting line theory. Differentiation with respect to roll rate yields the stability derivatives. A similar method is used for the r derivatives and the derivatives with respect to the actuator δ_a .

C. State-space Model

The final state-space model is assimilated from the various stability derivatives and other coefficients. The output is chosen to be a combination of roll rate and yaw rate which can be measured on-board with sensors. The system is given below.

$$\begin{bmatrix} \dot{\beta} \\ \dot{p} \\ \dot{r} \\ \dot{\phi} \end{bmatrix} = \begin{bmatrix} -0.7506 & 0 & -8 & 9.7505 \\ -8.106 & -6.7459 & 3.7592 & 0 \\ 24.9552 & -1.7593 & 0.0432 & 0 \\ 0 & 1 & 0.1106 & 0 \end{bmatrix} \begin{bmatrix} \beta \\ p \\ r \\ \phi \end{bmatrix} + \begin{bmatrix} 0 \\ -52.738 \\ 5.8369 \\ 0 \end{bmatrix} \delta_a$$

$$\begin{bmatrix} p \\ r \end{bmatrix} = \begin{bmatrix} 0 & 1 & 0 & 0 \\ 0 & 0 & 1 & 0 \end{bmatrix} \begin{bmatrix} \beta \\ p \\ r \\ \phi \end{bmatrix} + \begin{bmatrix} 0 \\ 0 \end{bmatrix} \delta_a \quad (4)$$

MATLAB is used for all computations and to simulate the system's time response. The poles of the system are found to be located at -7.7791 , $-0.1724 + 14.6195i$, $-0.1724 - 14.6195i$, and 0.6706 . There are two distinct real eigenvalues, one positive and one negative, and a complex conjugate pair with negative real part, indicating that the system is unstable in the spiral mode.⁵ In this mode, a small roll disturbance will cause the aircraft to spiral inward. Also, the aircraft oscillates in yaw due to the complex poles. Figure 3 shows the system's response to an initial disturbance given by $[\beta \mid p \mid r \mid \phi]^T = [0.1 \mid 0.1 \mid 0.1 \mid 0.1]^T$.

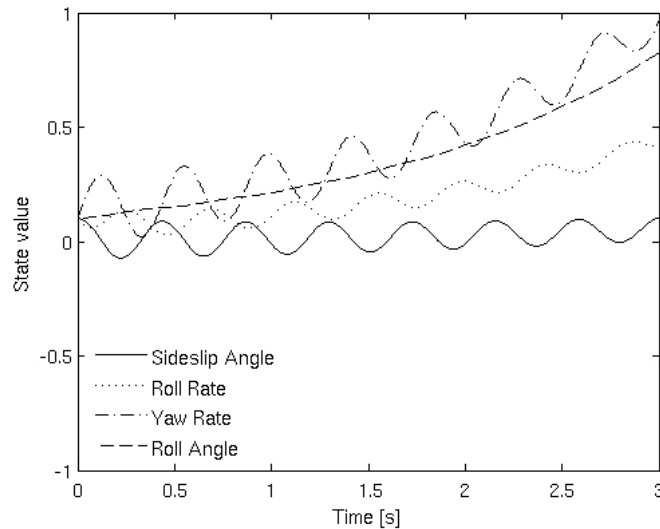


Figure 3. Response of the open loop system to an perturbed initial condition.

III. Control

We define the objective of the control system as the ability to recover from a perturbed initial condition within acceptable time and displacement bounds. An acceptable time limit for recovery for the MAV is three seconds. Because of the linearization procedure, there is a finite region around the linearizing point (zero) where the model is valid. One of the approximations is the small angle approximation, which is valid for angles less than approximately 17° . Thus, the requirement that all angles remain less than 17° will be used to define maximum overshoot and amplitude of oscillation. The response will be taken as the solution of the system with an initial condition of $[0.1 \mid 0.1 \mid 0.1 \mid 0.1]^T$. This is an approximation of the perturbed initial condition that the MAV might experience due to a wind gust.

Reachability describes the system's capability to reach an arbitrary state if it is given the correct input. It depends on the rank of the matrix $P = [B \mid AB \mid \dots \mid A^{n-1}B]$.⁹ If $\text{rank}(P) = n$, where n is the number of states, the system is completely reachable. The rank of P is found to be 4, which is n for this system. The system is therefore completely reachable. In a similar fashion, the observability of the system is a

measure of the ability to distinguish a given state from the zero vector. It is related to the rank of the matrix $Q = [C^T \mid A^T C^T \mid \dots \mid (A^{n-1})^T C^T]$. If $\text{rank}(Q) = n$, the system is completely observable. The rank of Q is also found to be 4, meaning that the system is completely observable.

A system may be controlled by adding state feedback.⁹ This means giving the system an input which depends on the state of the system. The input \mathbf{u} is then

$$\mathbf{u} = F\mathbf{v} - K\mathbf{x} \quad (5)$$

The new input is \mathbf{v} , where the matrix F relates \mathbf{v} to \mathbf{u} . The matrix K determines the relationship between \mathbf{x} and \mathbf{u} . The modified system is

$$\dot{\mathbf{x}} = (A - BK)\mathbf{x} + F\mathbf{v} \quad (6)$$

By selecting a proper K , the poles of the system can be selected so that the system will behave in a desired manner. The poles of the modified system are the eigenvalues of $(A - BK)$. It is observed that the roll rate p experiences the largest amplitude, and is therefore the most restrictive case. The settling time is defined as the time required for the solution to enter an envelope within 10% of the initial condition from the equilibrium point. The poles are successively changed until the maximum amplitude and settling time are within the acceptable tolerances defined above, and are $\mathbf{p} = [-2.65 \mid -11.0 + 0.6i \mid -11.0 - 0.6i \mid -32.0]$. The response to the perturbed initial condition is shown in Fig. 4.

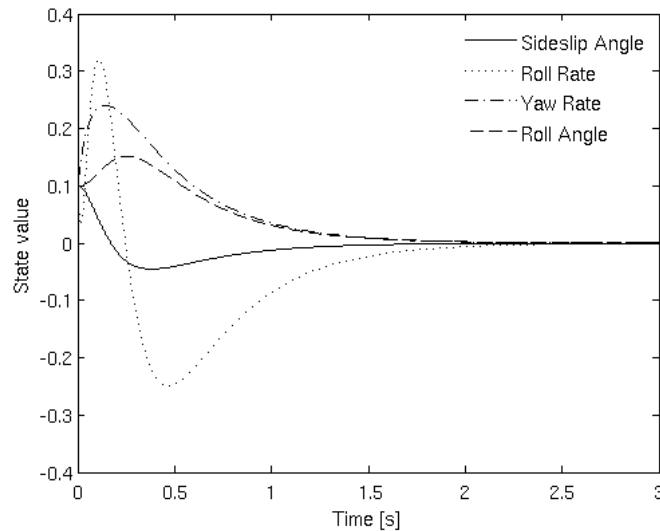


Figure 4. Response of the system with feedback controller to perturbed initial condition.

The system has a small amount of oscillation. One of the poles is much less than zero, which drives the system toward zero quickly. The other three have larger real parts, closer to zero. It is observed that when these poles are moved further to the left in the complex plane, the maximum amplitude of the oscillation increases. However, when the poles are moved close to zero, the maximum amplitude decreases but the settling time increases beyond the tolerance. The solution presented above represents a compromise on this issue.

If the output of the system does not include all of the states, it is impossible to implement a feedback controller directly because some or all of the states are unknown at any given time. This means that the input \mathbf{u} , given by Eq. (5), cannot be determined. To avoid this problem, a state observer is designed to estimate the states at any given time based on the outputs \mathbf{y} .⁹ The observer states $\hat{\mathbf{x}}$ are governed by the system

$$\begin{aligned} \dot{\hat{\mathbf{x}}} &= A\hat{\mathbf{x}} + B\mathbf{u} + L(\mathbf{y} - \hat{\mathbf{y}}) \\ \hat{\mathbf{y}} &= C\hat{\mathbf{x}} + D\mathbf{u} \end{aligned} \quad (7)$$

By defining the error as $\mathbf{e} \equiv \mathbf{x} - \hat{\mathbf{x}}$, a composite system can be created:

$$\begin{aligned} \begin{bmatrix} \dot{\mathbf{x}} \\ \dot{\mathbf{e}} \end{bmatrix} &= \begin{bmatrix} A - BK & BK \\ 0 & A - CL \end{bmatrix} \begin{bmatrix} \mathbf{x} \\ \mathbf{e} \end{bmatrix} + \begin{bmatrix} BF \\ 0 \end{bmatrix} \mathbf{v} \\ \mathbf{y} &= \begin{bmatrix} C & 0 \end{bmatrix} \begin{bmatrix} \mathbf{x} \\ \mathbf{e} \end{bmatrix} \end{aligned} \quad (8)$$

The poles of L should be far to the left on the complex plane so that the observer states will converge to the actual states quickly. Again, the values of the poles are changed iteratively until the desired performance is obtained. It is observed that some pole locations generate larger maximum amplitudes of β oscillation, while others lead to longer settling times. The poles which are found to produce the best response from the composite system are $\mathbf{q} = [-8.6 \mid -11.0 \mid -13.0 \mid -30.0]$. The response to the perturbed initial condition, where the initial values for the observer states are equal to those for the system, is shown in Fig. 5.

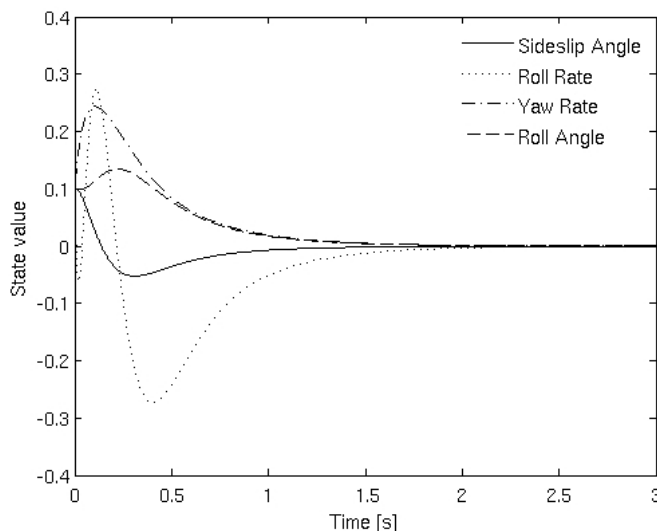


Figure 5. Response of the composite system to perturbed initial condition.

The composite system behaves in a nearly identical manner to the system without the observer, which is the goal of the observer. The error between the observer and the system is shown in Fig. 6. The error decays to zero in less than one second.

The control input required to recover from the initial perturbation is well within acceptable limits. Figure 7 shows that the the aileron deflection does not oscillate, and quickly damps to zero.

IV. Conclusions

Despite the lack of a vertical control surface, the MAV is controllable. A feedback controller and state observer have been designed which provide a sufficient response to a perturbed initial condition. The control system uses two rate gyros and actuates ailerons only. The four-state controller is simple enough to implement on an eight bit microcontroller flight computer. However, we are investigating simpler approaches to further reduce cost and requirements for on-board processing. Behavior of the longitudinal dynamics are also being investigated, which can be controlled by feedback to the elevons actuated collectively.

Acknowledgments

The research in this paper was partially supported by the NSF contract 427947 and the AFOSR contracts F49620-02-1-0176 and FA9550-05-1-0334. The authors would like to thank Philippe Geuzaine and Koen

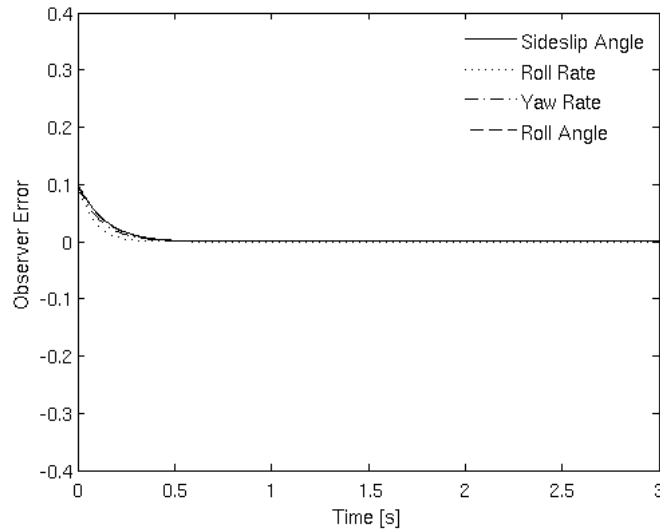


Figure 6. Response of the observer error to an initial error which is equal to the initial perturbation.

Hillewaert from CENAERO, Belgium for their assistance with the CFD simulations.

References

- ¹K. Mohseni, D. Lawrence, D. Gyllhem, M. Culbreth, and P. Geuzaine. Flow simulation around a micro air vehicle in a plume characterization scenario. AIAA paper 2004-6598, American Institute of Aeronautics and Astronautics, *3rd Unmanned Unlimited Technical Conference, Workshop and Exhibit*, September 20-22 2004.
- ²D.A. Lawrence, K. Mohseni, and R. Han. Information energy for sensor- reactive UAV flock control. AIAA paper 2004-6530, Chicago, Illinois, 20-23 September 2004. *3rd AIAA Unmanned Unlimited Technical Conference, Workshop and Exhibit*.
- ³J. Hall, K. Mohseni, D. Lawrence, and P. Geuzaine. Investigation of variable wing-sweep for applications in micro air vehicles. AIAA paper 2005-7171, American Institute of Aeronautics and Astronautics, *Infotech at Aerospace*, Arlington, VA, September 26-29 2005.
- ⁴D. Lawrence and K. Mohseni. Efficiency analysis for long-duration electric mavs. AIAA paper 2005-7090, AIAA Infotech@Aerospace, Arlington, Virginia, September 26-29 2005.
- ⁵Warren F. Phillips. *Mechanics of Flight*. John Wiley and Sons, Inc., Hoboken, NJ, 2004.
- ⁶Louis V. Schmidt. *Introduction to Aircraft Flight Dynamics*. American Institute of Aeronautics and Astronautics, Inc., Reston, VA, 1998.
- ⁷M.-S. Liou and C.J. Steffen Jr. A new flux splitting scheme. *Journal of Computational Physics*, 107:23–39, 1993.
- ⁸D. Gyllhem, K. Mohseni, D. Lawrence, and P. Geuzaine. Numerical simulation of flow around the Colorado micro aerial vehicle. AIAA paper 2005-4757, American Institute of Aeronautics and Astronautics, *35th AIAA Fluid Dynamics Conference and Exhibit*, Toronto, Canada, June 6-9 2005.
- ⁹William L. Brogan. *Modern Control Theory*. Prentice Hall, Upper Saddle River, NJ, 1991.

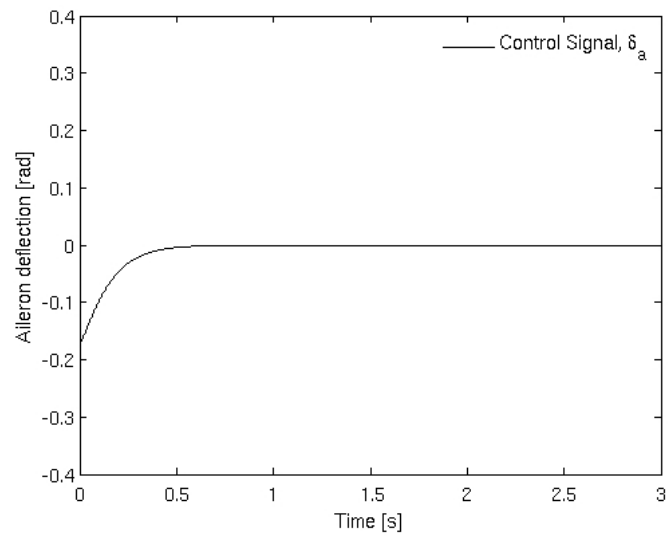


Figure 7. Control input required to recover from initial perturbation.